Brain Structure and Function
https://doi.org/10.1007/s00429-023-02614-1

ORIGINAL ARTICLE

Dopaminergic innervation at the central nucleus of the amygdala reveals distinct topographically segregated regions

Eric Casey[1,4] · María Elena Avale[1,2] · Alexxai Kravitz[3,4,5] · Marcelo Rubinstein[1,2]

Received: 29 October 2022 / Accepted: 16 January 2023

Abstract

The central nucleus of the amygdala (CeA) is involved in the expression of fear and anxiety disorders. Anatomically, it is divided into medial (CeM), lateral (CeL), and capsular (CeC) divisions. The CeA is densely innervated by dopaminergic projections that originate in the ventral periaqueductal gray/dorsal raphe (vPAG/DR) and the ventral tegmental area (VTA). However, whether dopamine (DA) exerts a homogenous control over the CeA or differentially regulates the various CeA subdivisions is still unknown. Here, we performed a neuroanatomical analysis of the mouse CeA and found that DAergic innervations from the PAG/DR and VTA constitute distinct, non-overlapping, pathways differing also in the relative expression of the dopamine transporter. By quantifying the distribution of DAergic fibers and the origin of DA inputs we identified two distinct regions in the CeL: a frontal region innervated by the VTA and vPAG/DR, a caudal region innervated only by the vPAG/DR, and three distinct regions in the CeC: fronto-dorsal innervated only by the VTA, fronto-ventral with sparse DAergic innervation, and a caudal region with low innervation from the vPAG/DR. In addition, we found that each region displays a distinct pattern of c-Fos activation following the administration of various DAeric drugs such as cocaine, SKF 38,393, quinpirole or haloperidol. In summary, we revealed unique properties of the DAergic pathways innervating the CeA, distinguishing six topographically segregated and functionally distinct regions. This unanticipated level of heterogeneity calls for more precise neuroanatomical specificity in future functional studies of the CeA.

Keywords Amygdala · Dopamine · Neuroanatomy · Periaqueductal gray · Ventral tegmental area

Introduction

The central nucleus of the amygdala (CeA) is a neural hub that integrates environmental and internal cues related to fear and anxiety and elicits conditioned behavioral responses. Studies in the CeA have gained considerable interest given its involvement in several pathological conditions such as anxiety disorders and drug addiction (Etkin et al. 2009; Tye et al. 2011; Koob and Volkow 2016; Koob 2008). The CeA is divided into three anatomical portions defined as medial (CeM), lateral (CeL) and capsular (CeC) (Olucha-Bordonau et al. 2015), each containing distinctive neuronal populations characterized by different molecular markers (McCullough et al. 2018), connectivity and functions (McCullough et al. 2018; Janak and Tye 2015; Kim et al. 2017).

The CeA contains neurons expressing either dopamine D1 (D1R) or D2 receptors (D2R) (Kim et al. 2017; De Bundel et al. 2016; Groessl et al. 2018) and is densely innervated by dopaminergic fibers (Groessl et al. 2018; Asan 1993). Functional studies have implicated dopamine (DA) in the

✉ Marcelo Rubinstein
mrubins@dna.uba.ar

1 Instituto de Investigaciones en Ingeniería Genética y Biología Molecular, Consejo Nacional de Investigaciones Científicas y Técnicas, Vuelta de Obligado 2490, 1428 Buenos Aires, Argentina

2 Departamento de Fisiología, Biología Molecular y Celular, Facultad de Ciencias Exactas y Naturales, Universidad de Buenos Aires, 1428 Buenos Aires, Argentina

3 Department of Anesthesiology, Washington University in St. Louis, St. Louis, MO 63108, USA

4 Department of Psychiatry, Washington University in St. Louis, St. Louis, MO 63108, USA

5 Department of Neuroscience and Biomedical Engineering, Washington University in St. Louis, St. Louis, MO 63108, USA

Published online: 03 February 2023

CeA with a variety of behaviors including impulse control (Kim et al. 2018), fear conditioning (De Bundel et al. 2016; Groessl et al. 2018; Greba et al. 2001; Guarraci et al. 1999, 2000), fear expression (Guarraci et al. 1999; Lamont and Kokkinidis 1998) and defensive behaviors (De la Mora et al. 2012; Casey et al. 2022). Despite that, the DAergic circuits that regulate the CeA have been poorly studied in comparison with striatal pathways, and their anatomy and connectivity remain mostly unknown.

DAergic innervation of the CeA originates mainly in neurons located in the ventral periaqueductal gray and dorsal raphe (vPAG/DR), as well as neurons present in the ventral tegmental area (VTA), respectively (Freedman and Cassell 1994; Hasue and Shammah-Lagnado 2002; Li et al. 2016). Although the anatomical distance between these inputs suggests that vPAG/DR → CeA and VTA → CeA circuits constitute independent pathways, it is unclear whether these innervations converge into the same CeA targets or whether they differentially regulate the various parts of the CeA. This gap in the current understating of how these circuits are organized constitutes a critical concern given the high diversity of neuronal types and functions within the CeA (Kim et al. 2017). In an effort to close this gap, here, we sought to study the innervation patterns of the vPAG/DR → CeA and VTA → CeA DAergic pathways into the different topographical regions of the CeA and also to determine whether these regions respond differently to the in vivo administration of DAergic compounds. To these goals, we performed a detailed neuroanatomical characterization of DAergic inputs at the CeA and revealed that vPAG/DR and VTA projections to the CeA are mostly non-overlapping pathways expressing different levels of the DA transporter (DAT). A careful analysis of DAergic innervation at the CeA allowed us to differentiate a fronto-dorsal, fronto-ventral and caudal region in the CeC, and a frontal and caudal region in the CeL. In addition, using an in vivo pharmacological approach in mice we demonstrated that these CeA subregions display unique patterns of c-fos activation following the systemic administration of DAergic drugs.

Results

DAergic innervations at the CeA

We first analyzed the distribution of DAergic fibers innervating the CeA and determined their relative density across the fronto-caudal extension of each division by tyrosine hydroxylase (TH) immunofluorescence. We found that the most densely innervated area of the CeA is the CeL, while the CeM showed only moderate innervation, and the CeC exhibited an even lower density of TH immunoreactive fibers (Fig. 1A, B). While we did not detect a fronto-caudal gradient of DAergic innervation in any division of the CeA (Fig. 1B), we did find a decreasing dorso-ventral gradient at frontal regions of the CeC (anterior to − 1.22 mm, Fig. 1C). Further analysis of fronto-dorsal and fronto-ventral regions of the CeC evidenced a fronto-caudal gradient only in the CeC (Supplementary Fig. 1). By dividing the CeA divisions according to the gradients described above, we found significant differences in the density of DAergic innervation at the diverse regions (Fig. 1D). Consistently, we found a similar distribution of fibers expressing the red fluorescent marker *tdTomato* in double transgenic mice carrying a $Dat^{IRES-Cre}$ *knockin* allele (Bäckman et al. 2006) and the Cre-inducible reporter gene Ai14 (Madisen et al. 2010), confirming the DAergic identity of these projections (Supplementary Fig. 2).

vPAG/DR DAergic neurons display limited expression of DAT

In contrast to the intense TH immunolabelling found in the CeA, immunohistochemistry performed using an antibody raised against the DA transporter (DAT) only showed weak signal in the CeA (Fig. 2A, left), suggesting that DAT levels in neurons innervating the CeA is relatively low. Then, we evaluated the presence of DAT in the two main DAergic inputs of the CeA and found that while DAT immunohistochemistry strongly labeled midbrain neurons from the VTA and substantia nigra compacta (SNc), (Fig. 2A middle), it was almost undetectable in neurons from the vPAG/DR (Fig. 2A right). To further confirm this result with a more sensitive approach, we evaluated the colocalization of DAT, using *tdTomato* as a reporter in $Dat^{+/IRES-Cre}$.Ai14 mice; and TH, using green immunofluorescence. We found that only half (49.1 ± 4.1%) of TH immunolabeled neurons in the vPAG/DR also expressed *tdTomato* (Fig. 2B, C), a number that could be even lower, because the presence of *tdTomato* in adult mice may be reporting earlier and transient *Dat* activation during development. By injecting fluorescent retrobeads (Lumafluor) in the CeA of those mice (Fig. 2D), we found that both *Dat* + and *Dat*- neurons were retrolabeled with retrobeads in the vPAG/DR, demonstrating that both types of DAergic neurons project to the CeA (Fig. 2E). Furthermore, while almost all neurons projecting from the VTA to the CeA coexpresed *Dat* and *Th*, the amount of retrolabeled TH + neurons expressing *Dat* in the vPAG/DR was significantly lower (Fig. 2E, F), demonstrating that CeA inputs from the VTA and the vPAG/DR differ substantially in their expression of DAT.

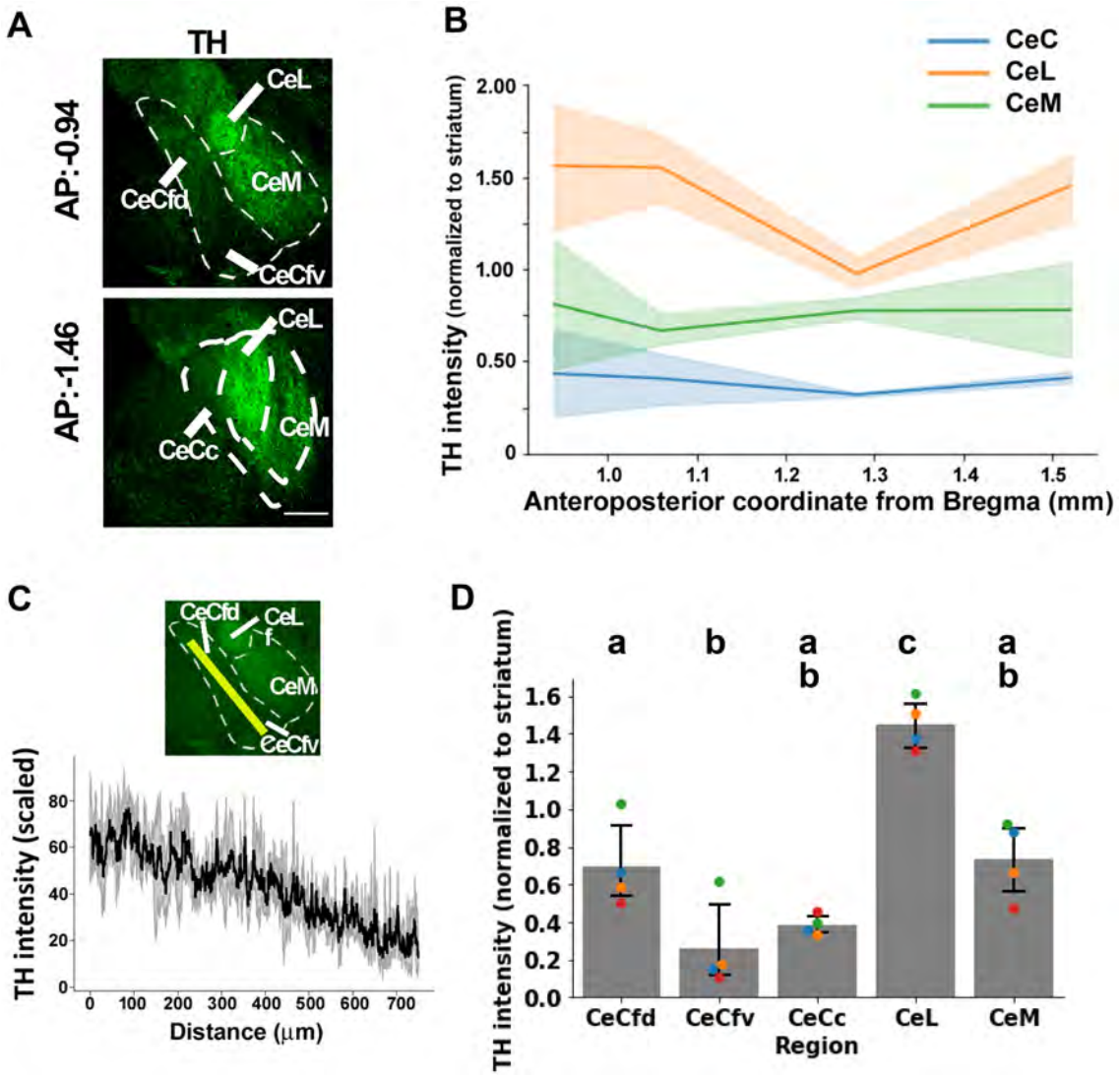

Fig. 1 Distribution of DAergic fibers in the CeA. **A** Representative histology of the CeA, according to Paxinos and Franklin (2008), of a *wild-type* mouse immunostained against TH. Upper row: frontal part of the CeA, from AP:-0.82 to AP:-1.06 mm (the example corresponds to AP:-0.94 mm); bottom row: caudal part of the CeA, from AP: − 1.22 to AP: − 1.70 (the example corresponds to AP: − 1.46 mm). **B** Quantification of TH immunofluorescence intensity across the fronto-caudal axis, for each division. Values are normalized to intensity in the dorsal striatum of the same coronal section. Significances inferred through Akaike information criterion (AIC) of nested models indicated significant effect of division, but not significant effect of fronto-caudal coordinate nor interaction ("Null model", AIC = 88.3; "TH ~ Division" model, AIC = 20.6; "TH ~ Division + Coordinate" model, AIC = 21.6; "TH ~ Division × Coordinate" model (with interaction), AIC = 24.4; $n = 4$ mice, 2–7 sections per mice). **C** Dorso-ventral gradient of DAergic fibers in the frontal CeC. Top: representative histology of the frontal part of the CeA immunostained against TH. Bottom: quantification of fluorescence intensity (in bits) through the transect marked by a yellow line in the top figure, the average values ± standard deviation corresponding to 4 slices from 3 different mice are shown**.** Linear regression indicated a significant negative slope; linear mixed model, Wald's test: Intercept, value = 67.1, $p < 0.001$; Slope, value = − 0.065, $p < 0.001$. **D** Quantification of intensity of TH immunofluorescence in different regions of the CeA; each dot indicates data from each mouse with values resulting from the average of 1–7 sections for each region, bars and errors indicate the mean ± 95% confidence interval for each region. Repeated measures ANOVA, $p < 0.0001$ ($n = 4$ mice). Post-hoc Bonferroni test is indicated; same letter indicates not-significant differences ($p > 0.05$) and different letters indicate significant differences ($p < 0.05$). CeL, lateral division of the central amygdala; CeCfd, capsular division of the central amygdala, frontodorsal part; CeCfv, capsular division of the central amygdala, frontoventral part; CeCc, capsular division of the central amygdala, caudal part; CeM, medial division of the central amygdala. Scale bars: 200 μm

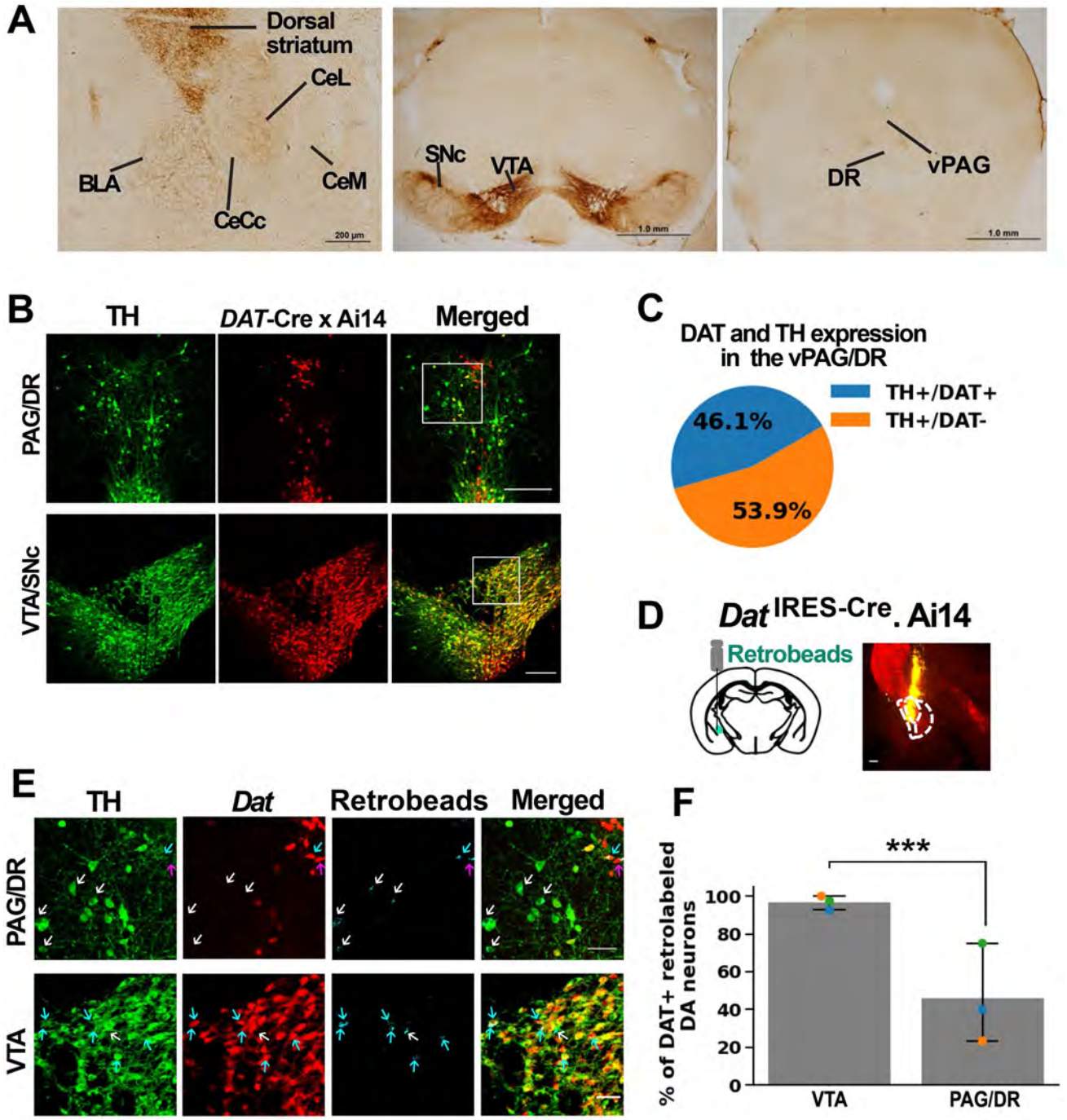

Fig. 2 vPAG/DR DAergic neurons display limited expression of DAT. **A** Immunohistochemistry against DAT on coronal sections containing the CeA (left), the VTA and SNc (center) and the vPAG/DR (right). **B–C** Colocalization of *Dat* (*tdTomato*) and TH (immunofluorescence) was analyzed in $Dat^{+/IRES-Cre}$.Ai14 mice. **B** Representative coronal sections. **C** Quantification; values represent the average percentage of neurons coexpressing *Dat* and TH or TH alone ($n=3$ mice). **D–F** Retrobeads were injected in the CeA of $Dat^{+/IRES-Cre}$.Ai14 mice and the colocalization of *Dat* (*tdTomato*) and TH (immunofluorescence) was analyzed in the retrolabeled neurons of the vPAG/DR and VTA. **D** Scheme of the surgery and representative histology at the injection site. **E** Magnifications of the squared areas in **B**, showing retro-labeled neurons (cyan). White arrows indicate examples of retrolabeled TH+/*Dat*- neurons; light blue arrows indicate retrolabeled TH+/*Dat*+neurons; pink arrows indicate retrolabeled TH-/*Dat*+neurons. **F** Percentage of *Dat*+neurons from all retrolabeled and TH+neurons, in the VTA and in the PAG/DR**.** Bootstrap with 10000 replicates, $p<0.0001$, $n=3$ mice). Scale bars: 200 µm (**A**, left and **B**); 1.0 mm (**A**, center and right); 50 µm (**E**)

Distinct DAergic innervations from the vPAG/DR and VTA to the CeA

The CeA receives DAergic inputs arriving from the VTA and the vPAG/DR (Freedman and Cassell 1994; Hasue and Shammah-Lagnado 2002; Li et al. 2016), but it was unclear whether both pathways converge in the same areas or rather assemble different circuits that control specific subdivisions of the CeA. To evaluate these two alternatives, we performed a double immunofluorescence study

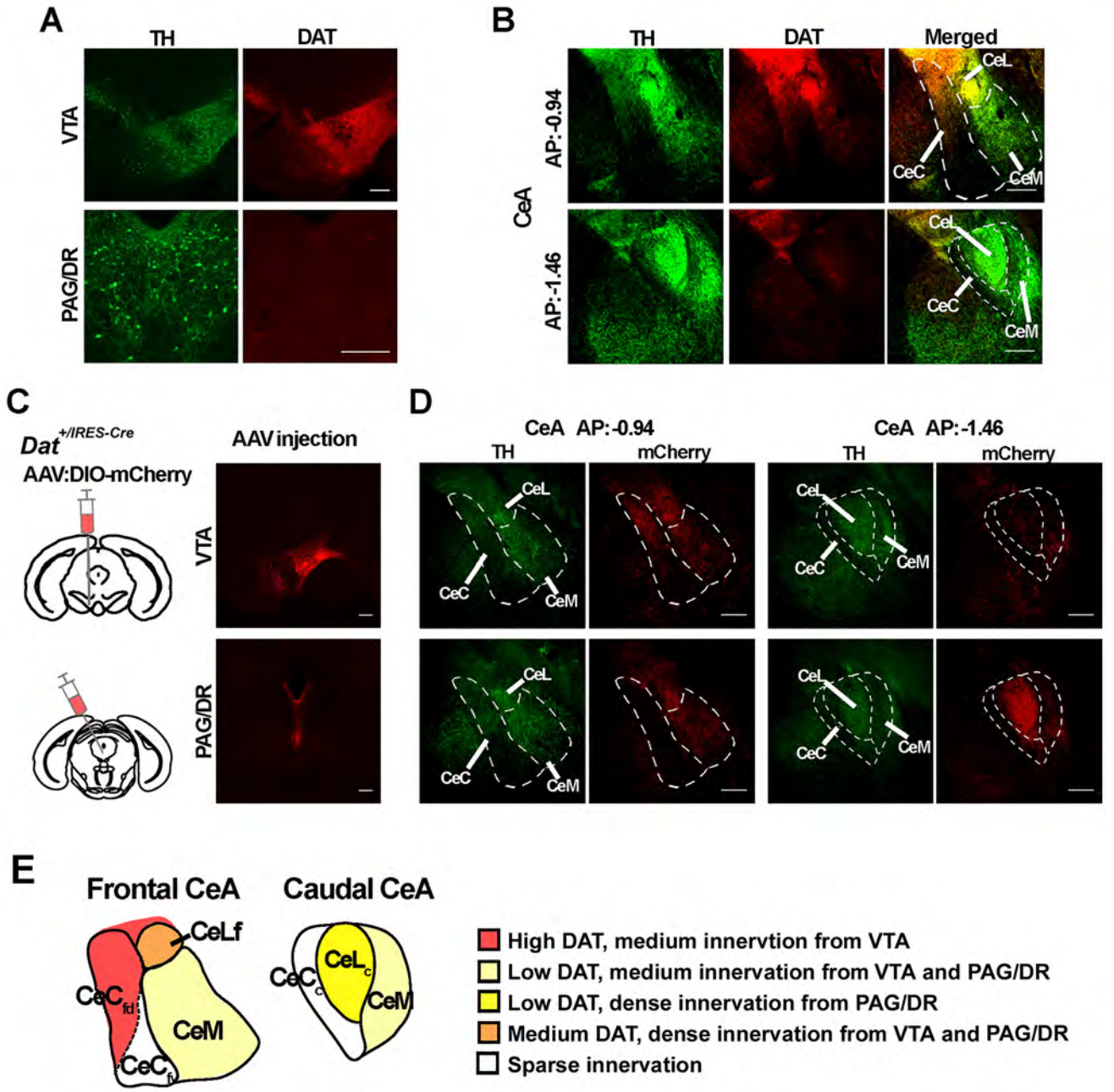

Fig. 3 DAergic inputs from the PAG/DR and VTA display distinct distributions in the CeA. **A**–**B** Immunofluorescence against TH (green) and DAT (red) in the VTA (**A**, top), the PAG/DR (**A**, bottom) and the CeA (**B**). **C** Representative coronal sections of a *Dat*$^{+/IRES-Cre}$ mouse brain injected with Cre-inducible ChR2-mCherry in the VTA (top) or the vPAG/DR (bottom), and **D** resulting labeling of fibers (red) in frontal (left) and caudal (right) CeA and immunofluorescence against TH (green). **E** Schematic depicting the distribution of DAergic fibers of each pathway in the CeA. The frontodorsal (fd) and frontoventral (fv) parts of the CeC are separated by dashed lines to highlight their different DAergic innervation content. CeLf, lateral division of the CeA, frontal part; CeLc, lateral division of the CeA, caudal part; CeCfd, capsular division of the CeA, frontodorsal part; CeCfv, capsular division of the CeA, frontoventral part; CeCc, capsular division of the CeA, caudal part; CeM, medial division of the CeA. Scale bars: 200 µm

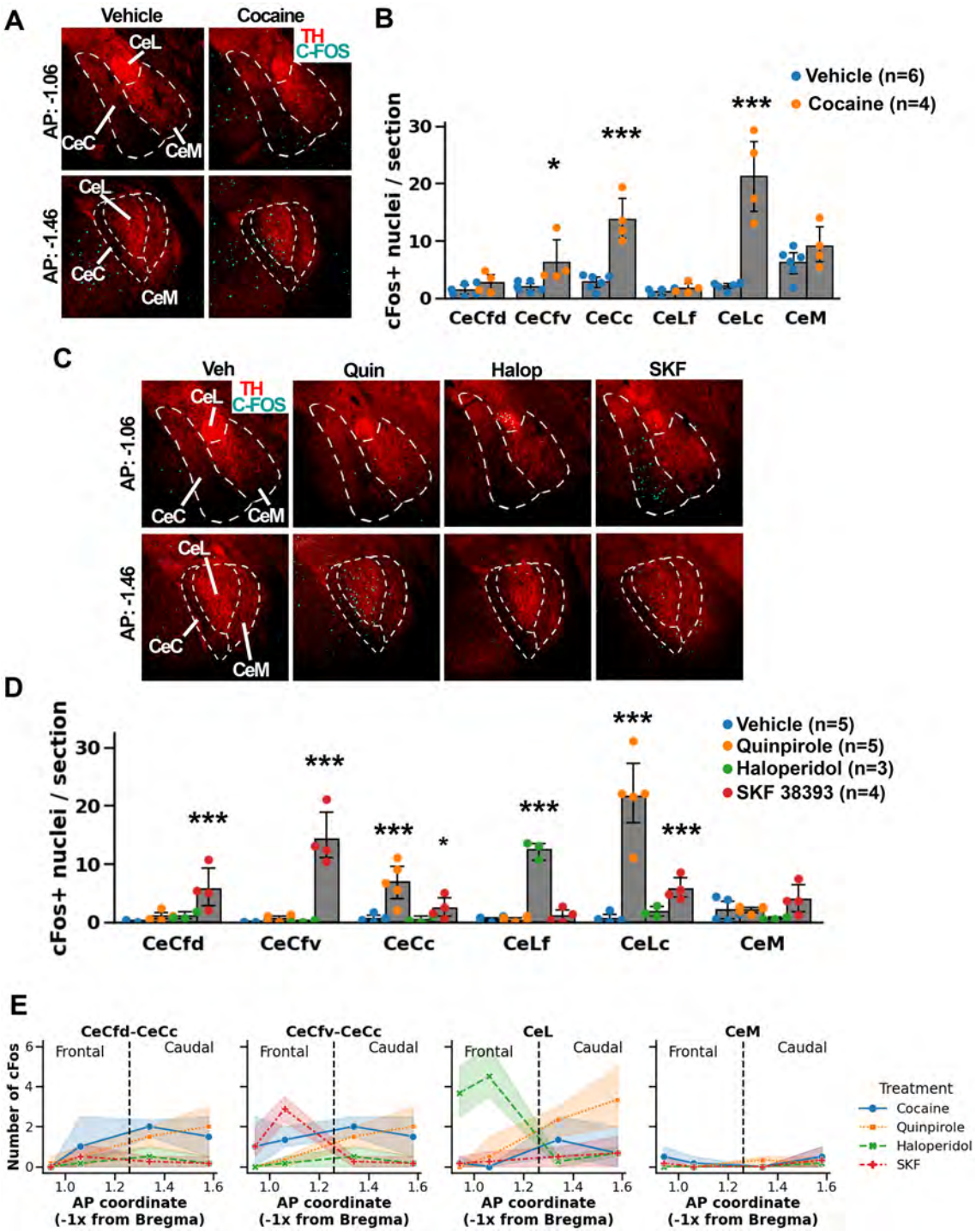

using antibodies against DAT and TH. We reasoned that, if innervation arriving from the VTA or the vPAG/DR were topographically segregated, we would detect a heterogeneous immunofluorescence distribution of DAT/TH signal ratios in the different regions of the CeA. Conversely, if both pathways were to converge into the different CeA regions, we would observe a homogeneous distribution of DAT/TH signal at the target sites. In agreement with the results reported above, inputs from the VTA showed strong labeling for both TH and DAT, while inputs from the vPAG/DR showed undetectable DAT (Fig. 3A). In support of the hypothesis of segregated circuits, we found that DAT/TH ratios were highly heterogeneous in the CeA: the frontal CeC has the highest DAT/TH ratio, while the caudal CeC, caudal CeL and CeM have considerably

◂**Fig. 4** Effect of DAergic drugs on neuronal activation in the CeA. **A**–**B** c-*Fos* activation in the CeA induced by saline (vehicle) or cocaine. **A** Representative frontal (top) and caudal (bottom) CeA sections showing immunofluorescence for TH (red) and c-FOS (cyan). **B** Quantification of c-FOS positive nuclei in the various CeA regions in mice receiving saline or cocaine. Generalized linear mixed model with negative Binomial distribution (link: log); likelihood-ratio test, Region × Drug: $\chi^2(5) = 32.1$, $p < 0.0001$; post hoc Scheffé test, statistical differences between drugs for each division are shown; Vehicle, $n = 6$; Cocaine, $n = 4$. **C**–**D** c-FOS expression in the CeA induced by saline (Veh), quinpirole (Quin), haloperidol (Halop) or SKF 38393 i.p. injections. **C** Representative frontal (top) and caudal (bottom) CeA sections showing immunofluorescence for TH (red) and c-FOS (cyan). **D** Quantification of c-FOS positive nuclei. Two-way generalized linear mixed model with Poisson distribution (link: log); likelihood-ratio test, Region × Drug $p < 0.0001$; post hoc Scheffé test, statistical differences between drugs for each division are shown; Vehicle, $n = 5$; Quinpirole, $n = 5$; Haloperidol, $n = 3$; SKF 38393, $n = 4$. **E** Number of c-Fos expressing cells per sampling area (shown in Fig. 5A across the fronto-caudal axis after injections of each drug, for each division (2 plots for the CeC highlight differences between Cefd and CeCfv). Each value indicates the mean ± 95% confidence interval across samples and mice; Cocaine, $n = 12$ samples per region and 24 for CeM, 3 mice; Haloperidol, $n = 10$–12 samples per region and 22 for CeM, 3 mice; Quinpirole, $n = 12$ samples per region and 24 for CeM, 3 mice; SKF 38393, $n = 10$–14 samples per region, 4 mice. $^*p < 0.05$, $^{**}p < 0.01$, $^{***}p < 0.001$

lower DAT/TH ratios. In turn, the frontal CeL showed intermediate DAT/TH ratios (Fig. 3B and Supplementary Table 1). To further confirm these results, we labeled *Dat*-expressing neurons with a red fluorescent marker by stereotaxic injections of adeno-associated viral (AAV) particles expressing a Cre-inducible *mCherry* reporter into the vPAG/DR or VTA of $Dat^{+/IRES-Cre}$ mice (Fig. 3C). The *mCherry* fluorescent fibers arriving at the CeA from the vPAG/DR were qualitatively and quantitatively analyzed in both brain hemispheres since the AAV injections were delivered medially, whereas those injected unilaterally into the VTA were analyzed in the ipsilateral CeA since they showed considerably more labeling than the contralateral CeA. This analysis revealed two different innervation patterns. The Cre-inducible *mCherry* AAV particles injected into the VTA of $Dat^{+/IRES-Cre}$ mice labeled fibers in the frontal part of the CeC (AP: − 0.82 mm to AP: − 1.06 mm), and only a sparse array of fibers in the caudal part of the CeL/CeC (AP: − 1.22 mm to AP: − 1.70 mm) (Fig. 3D, top; Supplementary Fig. 3, left; Supplementary Table 2 and Supplementary Table 3). In contrast, injections of the same AAV into the vPAG/DR of $Dat^{+/IRES-Cre}$ mice labeled a dense array of fibers innervating the caudal portion of the CeL but not the frontal CeC (Fig. 3D, bottom; Supplementary Fig. 3, left; Supplementary Table 2 and Supplementary Table 3). In turn, the frontal part of the CeL (AP:-0.82 mm to AP:-1.06 mm) and the CeM were moderately labeled with fibers projecting from both the VTA and vPAG/DR (Fig. 3D; Supplementary Fig. 3, left; Supplementary Table 2 and Supplementary Table 3). These results are also consistent with data from the Allen Mouse Brain Connectivity Atlas (Oh et al. 2014) showing *Dat* and *Th* expressing projections from the VTA and vPAG/DR to the CeA (Supplementary Fig. 4). Together, these results reveal the existence of the following two distinct DAergic pathways innervating the CeA: (1) PAG/DR neurons projecting mainly to the caudal CeL and CeM that display low DAT levels (Fig. 3E) and (2) VTA neurons projecting mainly to the frontodorsal CeC expressing high DAT levels (Fig. 3E). Interestingly, both pathways seem to overlap in the frontal part of the CeL (moderated levels of DAT) and in the CeM (low DAT levels) (Fig. 3E). In addition, our analysis of the DAergic innervation allowed us to differentiate between a fronto-dorsal, a fronto-ventral and a caudal region in the CeC (CeCdf, CeCfv and CeCc, respectively) and a frontal and a caudal region in the CeL (CeLf and CeLc, respectively) (Fig. 3E).

CeA regions defined by their type of innervation are differentially activated upon the in vivo administration of DAergic drugs

We, next, evaluated how the CeA subregions described above respond to the in vivo administration of DAergic compounds with different pharmacological profiles, by following the activation of the immediate early gene *c-fos* as a functional proxy readout. We found that the indirect mixed D1/D2R DA agonist cocaine (20 mg/kg, i.p.) increased the number of c-FOS + nuclei only in the caudal part of the CeL and the caudal and frontoventral regions of the CeC (Fig. 4A, B). Similarly, the D2R-like agonist quinpirole (1 mg/kg, i.p.) increased the amount of c-FOS + nuclei exclusively in the caudal part of the CeL and the CeC, but not in the CeM or any other frontal region of the CeA (Fig. 4C, D). In contrast, the D2R-like antagonist haloperidol (0.3 mg/kg, i.p.) increased c-FOS immunoreactivity only in frontal CeL neurons (Fig. 4C, D). Finally, the D1R-like agonist SKF 38,393 (4 mg/kg, i.p.) strongly increased the number of c-FOS + nuclei in the fronto-ventral part of the CeC and, to a lesser extent, in the fronto-dorsal CeC, caudal CeC and caudal CeL (Fig. 4C, D). Analysis of c-FOS expression across the antero-posterior axis of the CeA further highlighted the existing differences in regions of the same division (Fig. 4E).

While these results imply that distinct CeA regions are differentially activated by DAergic compounds, the identification of distinct areas using a pre-conceived anatomical compartmentalization of the CeA could be somewhat biased. For example, if there were different patterns of activation in the CeM across its fronto-caudal axis, this method would not detect them simply because we did not delimit different regions in the CeM (Fig. 3E). To overcome this limitation, we sought to further analyze these responses using

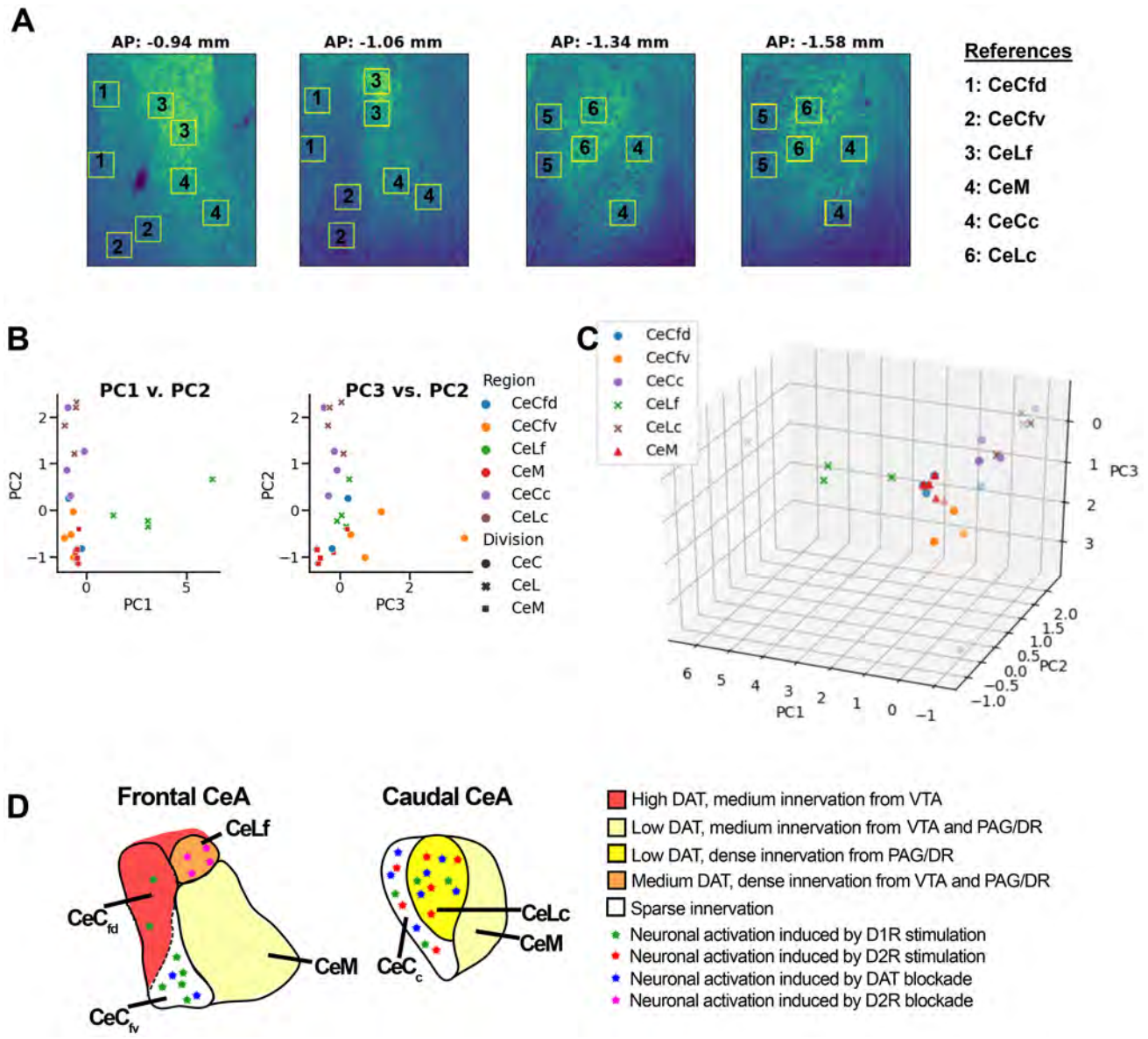

Fig. 5 Functional neuroanatomy of DAergic neurotransmission in the CeA reveals six topographically segregated regions. **A** Representative CeA coronal sections indicating the areas used for the principal component analysis (PCA). **B**–**C** PCA of the average number of c-Fos expressing cells in each sample (average of 3–4 mice per sample) after injections of cocaine, SKF 38393, quinpirole and haloperidol. 2D (**B**) and 3D (**C**) scatter plots show that samples in the same region tend to cluster together. **D** Schematic of the CeA summarizing the distribution of DAergic fibers and effect of DAergic drugs. CeLf, lateral division of the CeA, frontal part; CeLc, lateral division of the CeA, caudal part; CeCfd, capsular division of the CeA, frontodorsal part; CeCfv, capsular division of the CeA, frontoventral part; CeCc, capsular division of the CeA, caudal part; CeM, medial division of the CeA

an unsupervised learning method that avoids preconceived biases regarding CeA region delimitations. To this end, we delimited two 80 × 80 µm squares per region in each of the four antero-posterior selected coordinates (Fig. 5A), and the location of these areas remained fixed for all mice. This procedure allowed us to analyze results in four samples per region except the CeM, which had eight samples since this division was not split into frontal and caudal regions (Fig. 5A). Then, we calculated in every sample the level of c-Fos expression induced by each drug, and multivariate responses (c-Fos activity for every drug) corresponding to each sample were analyzed following a principal component analysis (PCA). We found that the three first principal components (PC1, PC2 and PC3) explained over 90% of the variance of the data, mostly influenced by haloperidol, quinpirole and SKF 38,393, respectively (Supplementary Table 4). Scatterplots of principal component values revealed that samples corresponding to regions identified

by their DAergic innervation tended to group together: CeLf samples grouped in a cluster with the highest PC1 values, CeCc and CeLc samples clustered with the highest PC2 values, and CeCfv samples clustered with the highest PC3 values. Finally, CeM and CeCfd samples, mostly clustered together at the lowest values of each component (Fig. 5B, C). Interestingly, the results obtained when using an unsupervised learning algorithm to analyze drug-induced c-Fos activation along the various CeA regions are coincidental with those found after analyzing the distinct patterns of DAergic innervation. Altogether, these results reveal that each CeA region displays a unique pattern of activation when treated with pharmacological compounds that affect DAergic neurotransmission: the frontal part of the CeL was activated exclusively by D2R-blockade, the fronto-dorsal part of the CeC was activated exclusively by D1R stimulation (although this effect was subtle and for this reason it grouped with the CeM in the PCA), the fronto-ventral CeC was activated by D1R stimulation and DAT blockade, and the caudal CeC and caudal CeL were activated by D1R stimulation, DAT blockade and D2R stimulation. Differently, the CeM did not show any increase in c-FOS following any of the pharmacological manipulations used in this study, compared with saline injections (Fig. 5D). In summary, our results demonstrate that the DAergic innervation into the CeA features six regions in this area, each of which exhibits a particular activation profile in response to the in vivo systemic administration of DAergic compounds.

Discussion

Although DA innervation at the CeA has been largely studied (Groessl et al. 2018; Freedman and Cassell 1994; Hasue and Shammah-Lagnado 2002; Li et al. 2016), it remains unclear whether inputs arriving from the vPAG/DR and the VTA converge into the same CeA regions or rather constitute separate pathways that regulate the CeA with distinct properties. In this work, we demonstrate that the vPAG/DR and the VTA pathways assemble two different, mostly non-overlapping, circuits (Fig. 3). Furthermore, the topographical organization of DA fibers impinging the CeA allowed us to distinguish several regions among the three classical divisions of the CeA, each of which showing a specific pattern of c-fos activation following the systemic administration of DAergic drugs to live mice (Figs. 4 and 5). Together, these results suggest that vPAG/DR and VTA modulate distinct subsets of topographically segregated CeA neurons which are likely involved in different, although not necessarily unrelated, functions.

Our evidence for the topographical segregation of VTA and vPAG/DR fibers into the CeA was initially based on a relative quantitative immunofluorescence determination of DAT and TH. However, this analysis assumes that projections from these nuclei are homogenous regarding the levels of TH and DAT present in the individual neurons. For example, we found that the VTA displayed much higher DAT levels than the vPAG/DR, but VTA neurons with low DAT levels have also been documented elsewhere (Lammel et al. 2008). Although our retrograde labeling experiment showed intense tdTomato signal in almost all VTA DAergic neurons projecting to the CeA (Fig. 2E, F), *Dat* expression levels in this group of neurons could be heterogeneous considering that even a single molecule of *Dat*-activated Cre can promote expression of the reporter gene. Similarly, *Dat* positive and *Dat* negative DAergic neurons of the vPAG/DR could also innervate the CeA in a heterogeneous manner. In an effort to circumvent this issue, we performed an anterograde tracing experiment with genetic specificity which allowed us to confirm the topographical segregation indicated previously in our immunofluorescence study (Fig. 3D, Supplementary Fig. 3).

Another caveat to consider is that the TH antibody used in this study not only labels DA neurons but also noradrenergic and adrenergic inputs arriving to the CeA (Asan 1993, 1997; Gu et al. 2020). However, the accuracy of the quantification of DAergic fibers using TH immunolabeling would only affect the CeM, as adrenergic and noradrenergic fibers are scarce in the CeC and CeL (Asan 1993, 1997). In addition, the contribution of other catecholaminergic fibers would be minor since the vPAG/DR and VTA account for 95% of the DAergic inputs to the CeA (Hasue and Shammah-Lagnado 2002).

Classically, it has been established that DA reuptake by DAT is a fundamental mechanism for terminating DAergic neurotransmission, and accordingly, the presence of DAT has been largely recognized as a marker of DAergic neurons. However, here we have demonstrated that DAergic vPAG/DR neurons have atypically low DAT levels compared to those found in midbrain DAergic neurons. Similarly, limited DAT expression has been reported in VTA neurons projecting to the prefrontal cortex, nucleus accumbens medial shell and core and basolateral amygdala (Lammel et al. 2008). The lower levels of DAT observed in the PAG/DR is likely the consequence of an all or nothing *Dat* expression level in each individual neuron, as we observed in $Dat^{+/IIRES-Cre}$. Ai14 mice in which only half of TH positive neurons express *Dat*. However, the lower intensity of DAT immunostaining found in the CeL (Fig. 2A and Fig. 3B) compared with that shown by the reporter *tdTomato* in $Dat^{+/IRESCre}$.Ai14 mice (Supplementary Fig. 2) suggests that even neurons with transcriptionally active *Dat* express this gene at much lower levels than canonical DAergic neurons. The functional meaning of low DAT levels in the time-course of DAergic neurotransmission in the CeA should be further investigated in future studies, together with the effects of psychostimulants such

as amphetamine and cocaine (Giros et al. 1996; Jones et al. 1998).

The comparison of different Cre-driver mouse lines capable of targeting DA neurons is of high interest for a wide community of neuroscientists. In general, DAT-Cre mice have shown to be more selective than TH-Cre mouse lines to target DA neurons in the VTA (Stamatakis et al. 2013; Lammel et al. 2015; Stuber et al. 2015) and in the vPAG/DR (Cardozo Pinto et al. 2019). However, DAT-Cre lines were reported to have reduced penetrance in the VTA (Stuber et al. 2015) due to reduced *Dat* expression in specific populations of VTA DAergic neurons (Lammel et al. 2008; Blanchard et al. 1994). In agreement with the heterogeneous presence of DAT in VTA neurons, our results also show that ~ 50% of the DAergic neurons of the vPAG/DR, assessed by TH staining, coexpress DAT or coexpressed DAT during development, indicating a limitation of DAT-Cre lines to target DAergic neurons. Of note, given that we used a Cre-reporter mouse line (Bäckman et al. 2006) instead of viral vectors-mediated gene delivery, the incomplete penetrance we show in our study cannot be attributed to a partially efficient transduction rate. In addition, since the expression of tdTomato in the Ai14 line can be due to a transient expression of Cre during development, the actual percentage of neurons expressing *Dat* in adulthood could be even lower. However, it should be noted that *Dat* is expressed at some level in the vPAG/DR during adulthood, as vPAG/DR was labelled after viral delivery of a Cre-inducible *mCherry* reporter in adult DAT-Cre mice (Fig. 3C). In addition, we also noticed a population of *Dat* expressing neurons with undetectable TH, which were labeled with retrobeads injected in the CeA (Fig. 2B–E). Those DAT + and TH- neurons were small sized, rounded/oval shaped and located near the aqueduct of Sylvius, as previously described (Meloni 2006). Of note, neurons with those characteristics have been proposed to be DAergic and to express low *Th* levels, as found in *Th*-GFP and *Pitx3*-GFP mouse lines (Dougalis et al. 2012).

The detailed molecular neuroanatomical study performed here sheds light on the intricate organization of the CeA, the complexity of the DAergic innervation that each CeA subdivision receives and their heterogeneous responses to DA. Although the CeA is classically divided in CeC, CeL and CeM, the segregated DAergic innervation and the effect of DA compounds revealed a compartmentalized organization in which three regions in the CeC (frontodorsal, frontoventral and caudal) and two in the CeL (frontal and caudal) are distinguished (Fig. 5D). This finding is particularly relevant because most functional studies performed to date have focused in caudal regions of the CeA and studied together the CeC and CeL, as if they were a single nucleus. This simplification has limited the study of amygdalar circuits and their implications in emotional behaviors. For example, the role of D2Rs in the CeA seems to be controversial, with reports suggesting both anxiogenic (Greba et al. 2001; Guarraci et al. 2000) as well as anxiolytic (De Bundel et al. 2016; De la Mora et al. 2012; Casey et al. 2022) effects. Interestingly, our results show that frontal and caudal CeL display opposite responses to D2R stimulation and blockade (Fig. 4E, CeL), suggesting that small variations when placing stereotaxic-guided cannulas into the CeA may lead to different behavioral results and, therefore, seemingly diverging conclusions about the role of D2R in the CeA. Thus, this work highlights the need for more precise approaches to dissect the functional role of regions and particular neuronal populations of the CeA and also calls for a cautious interpretation of the current available data.

Methods

Mice husbandry

$Dat^{+/IRES-Cre}$ (Bäckman et al. 2006), Ai14 (Madisen et al. 2010) and *wild-type* mice were maintained in a C57BL/6 J background. Mice were housed in ventilated cages under controlled temperature and photoperiod (12 h light/12 h dark cycle, lights on from 7:00 AM to 7:00 PM), with tap water and laboratory chow available ad libitum, and separated by sex. All the experiments were performed on mice of both sexes and older than 8 weeks. All procedures were approved by the Institutional Animal Care and Use Committee of INGEBI-CONICET and followed the Arrive Guidelines, and the Guide for the Care and Use of Laboratory Animals (National Research Council 2011).

Stereotaxic surgeries

Mice were anesthetized with ketamine (100 mg/kg; i.p.) and xylazine hydrochloride (10 mg/kg; i.p.). A 10 µl Hamilton syringe connected with a 36-gauge metal needle was used to infuse adeno associated viral vectors or retrobeads using a microsyringe pump at 0.1 µl/min. All stereotaxic coordinates were in relation to the Bregma according to Paxinos and Franklin (2008); for the CeA: anterior–posterior, − 1.5 mm; medial–lateral, + / − 3.0 mm; dorsal–ventral, − 4.9 mm; for the VTA: anterior–posterior, − 3.1 mm; medial–lateral, + / − 0.4 mm; dorsal–ventral, − 4.5 mm; for the PAG/DR: anterior–posterior, − 4.1 mm; medial–lateral, − 1.8 mm; dorsal–ventral, − 2.1 mm, angle: 20° (to avoid the aqueduct). Following infusion, the needle was kept at the injection site for 5 min, and then slowly withdrawn to half way, kept there for 2 more min and then

slowly withdrawn outside the brain. Skin was sutured, and local anesthesia (lidocaine gel) was applied followed by the analgesic flunixin meglumine (5 mg/kg, s.c.). Mice were maintained on a regulated warm pad and monitored until recovery from anesthesia. For retrograde tracing, 0.3 µl of green retrobeads (Lumafluor, Green Retrobeads IX) were injected in a 1:4 dilution of the commercial stock in NaCl 0.9%. For anterograde tracing experiments, pAAV-Ef1a-DIO-hChR2(H134R)-*mCherry*-WPRE-pA, serotype 2 (5.2×10^{12} viral particles/ml, UNC Vector Core) were injected into the VTA/SNc (0.3 µl) or the PAG/DR (1.0 µl) of compound $Dat^{+/IRES-Cre}$.Ai14 mutant mice.

Drug administration and c-FOS detection

All drugs were dissolved in NaCl 0.9% to reach a concentration such that the injected i.p. volume was 0.1 ml per 10 g of mouse weight. Experiments evaluating cocaine effects were performed separately from those evaluating quinpirole and haloperidol, and because of that they were not included in the same statistical analysis. Vehicle (NaCl 0.9%), cocaine hydrochloride (20 mg/kg; Sigma), quinpirole (1 mg/kg; Sigma), haloperidol (0.3 mg/kg; Tocris) or SKF 38,393 (4 mg/kg; hydrobromide; Tocris) were injected i.p.. Mice were left in their home cage and 90 min later were perfused for tissue fixation and histology.

Perfusion and histology

Transcardiac perfusion was performed with 5 ml of phosphate buffered saline (PBS, 0.9% NaCl, 2.7 mM KCl, 10 mM K_2HPO_4, 2 mM KH_2PO_4, pH 7.5) followed by 50 ml of paraformaldehyde 4% in PBS and brains were removed and post-fixed in the same solution at 4 °C for 12–16 h. Brains were sectioned at 40 µm on a vibratome (Leica) and used immediately or stored at − 20 °C in a solution containing 30% (v/v) ethylene glycol, 30% (v/v) glycerol and PBS, until they were processed for immunofluorescence. Immunolabeling was performed as follows: free-floating sections were rinsed three times for 10 min in PBS and then incubated for 16 h at 4 °C in primary antibody solution with normal goat serum 2% (w/v), Triton X-100 0.3%, in PBS. The following primary antibodies were used: rabbit anti-TH (1:2,000; Millipore, AB5935), chicken anti-TH (1:1,000; Abcam, AB76442), rabbit anti-C-FOS (1:500, Santa Cruz Biotechnology, SC-52), rabbit anti-dsRed (1:500; Clontech, 632,496), rat anti-DAT (1:500, Millipore, MAB369). After incubation with a primary antibody, sections were rinsed twice for 20 min in PBS and then incubated for 2 h at room temperature with goat or donkey Alexa-488 or Alexa 555 coupled secondary antibody 1:1000 in Triton X-100 0.3% in PBS. Finally, sections were rinsed twice for 20 min in PBS and mounted with Vectashield (Vector Labs) for confocal microscopy or glycerol 50% (v/v) in PBS for fluorescence and bright field microscopy.

Microscopy and images analysis

Confocal images for co-expression analysis (Fig. 2) were obtained using a Leica Confocal TCS-SPE microscope. Co-expression was manually quantified using the tool "Cell Counter". Images for c-FOS quantification by anatomical region, innervation analysis, DAT and TH intensities measurements and anterograde tracing were obtained by fluorescence microscopy. Images were analyzed with the Fiji platform (Schindelin et al. 2012) of the ImageJ software (Rueden et al. 2017). Coronal sections from AP: -0.94 to AP: -1.06 mm for frontal regions of the CeA and sections from AP: -1.22 to AP: -1.58 mm for caudal regions of the CeA were analyzed. Borders between CeA divisions were established according to Paxinos and Franklin, 3rd edition (Paxinos and Franklin 2008), and further fronto-caudal borders are shown in Supplementary Fig. 5, as also used in ref. (McCullough et al. 2018).

Analysis of TH intensities, DAT intensities and DAT/TH ratios (Fig. 1B–D, Supplementary Table 1) were obtained as follows: regions from CeA, dorsal striatum and medial amygdaloid nucleus posterodorsal (MePD) were delimited and average intensities for TH and DAT channels were calculated using the tool "Measure". MePD was found to have considerable low signal for TH and DAT and was considered as background signal. For each section, MePD signal (background) was subtracted from values of other areas and then values from each CeA region was relativized to dorsal striatum values. Data of the same region from different slices were averaged to obtain intensity values shown in Fig. 1 and Supplementary Table 1. For each slice, normalized DAT values were divided by normalized TH values, and DAT/TH values of the same region from different sections were averaged to obtain DAT/TH ratios shown in Supplementary Table 1.

For Fig. 4B, D, cell number was semi-automatically quantified with the tool "Analyze particles" after manually delimiting the region of interest. For statistics, the number of cells in each nucleus was obtained adding the values of the corresponding nucleus for each of all sections, and the number of sections added was later used as offset in the Statistical analysis. For graphs, the mean of cells between sections was calculated for each nucleus.

For Figs. 4E and 5, images were automatically processed using Python with the libraries Numpy and SciPy. Between three to four coronal sections of each mouse, corresponding to AP 0.94, 1.06, 1.34 and 1.58 mm from Bregma, were analyzed. For each coronal section of every mouse, two 6400 μm^2 squares were delimited

in each region using images of TH histology (Fig. 5A) and without checking for c-Fos immunolabelling, to avoid bias. Images were read as Numpy arrays and transformed to binary such that only values above the 95.5 percentile were 1 and any other value was 0. For each sample, particles above the threshold were identified and labeled and particles of size above 30 pixels were quantified. Importantly, the location of the samples at each coronal section were the same for every mouse, and were manually chosen to minimize spanning multiple regions due to slight variations between images (the code provided in the section "Code and accessibility" displays the chosen samples for all the images used in this analysis); this procedure allowed us to calculate the average number of c-Fos positive nuclei across mice for each drug and sample to perform the principal component analysis with the pharmacological profile of each sample (Fig. 5B, C). For Fig. 4E, the average between samples of each region was first calculated for each mouse to avoid overestimating the amount of independent observations, and then the average and 95% confidence interval across mice for each drug was plotted.

Statistical analysis

All data represent the mean ± 95%CI and were graphed using Python (libraries matplotlib and seaborn). Statistical analysis were performed in Python (packages numpy, pingouin, statsmodels and sklearn) for Figs. 1, 2 and 5 or R Studio (libraries glmmTMB and lsmeans) for Fig. 4. The statistical analysis is indicated in the Figure legends. Results of Fig. 2F were analyzed using bootstrap instead of paired t-test because the data was neither normally distributed nor showed homoscedasticity. Discrete data of Fig. 4B and D were analyzed using a generalized linear mixed model (GLMM) with Poisson error structure (link: loggit) or Negative-binomial error structure when data had overdispersion. Assumptions for the GLMM were evaluated assessing the absence of patterns in Pearson's residuals graph and calculating the dispersion parameter to assess subdispersion or overdispersion. The principal component (Fig. 5B, C) analysis was performed using the average number of c-Fos positive nuclei of each sample between mice for each drug (columns) and sample (rows). Data was centered for each feature (drug) before to applying the Singular Value Decomposition of the PCA, but it was not scaled because the variable (amount of c-Fos expressing neurons) was the same across features. Principal components across drugs were calculated and used to plot scatter plots of each sample.

Supplementary Information The online version contains supplementary material available at https://doi.org/10.1007/s00429-023-02614-1.

Acknowledgements This work was supported by grants from the Agencia Nacional de Promoción Científica y Tecnológica, Argentina (M.R.) and a doctoral fellowship from Consejo Nacional de Investigaciones Científicas y Técnicas (CONICET), Argentina (E.C.).

Author contributions MR, MEA, AK, and EC designed research; MEA and EC performed research; MR and EC analyzed data; M.R. and E.C. wrote the paper.

Funding Agencia Nacional de Promoción Científica y Tecnológica, PICT-2018-01358

Data availability All data presented in this paper and codes for plotting and statistical analysis can be accessed at https://github.com/casey-e/Casey-et-al-2022-b.

Declarations

Conflict of interest The authors declare no competing financial interests.

References

Asan E (1993) Comparative single and double immunolabelling with antisera against catecholamine biosynthetic enzymes: criteria for the identification of dopaminergic, noradrenergic and adrenergic structures in selected rat brain areas. Histochemistry 99:427–442

Asan E (1997) Ultrastructural features of tyrosine-hydroxylase-immunoreactive afferents and their targets in the rat amygdala. Cell Tissue Res 288:449–469

Bäckman CM, Malik N, Zhang Y, Shan L, Grinberg A, Hoffer BJ et al (2006) Characterization of a mouse strain expressing Cre recombinase from the 3′ untranslated region of the dopamine transporter locus. Genesis 44:383–390

Blanchard V, Raisman-Vozari R, Vyas S, Michel PP, Javoy-Agid F, Uhl G et al (1994) Differential expression of tyrosine hydroxylase and membrane dopamine transporter genes in subpopulations of dopaminergic neurons of the rat mesencephalon. Mol Brain Res 22:29–38

Cardozo Pinto DF, Yang H, Pollak Dorocic I, de Jong JW, Han VJ, Peck JR et al (2019) Characterization of transgenic mouse models targeting neuromodulatory systems reveals organizational principles of the dorsal raphe. Nat Commun 10:4633

Casey E, Avale ME, Kravitz A, Rubinstein M (2022) Partial ablation of postsynaptic dopamine D2 receptors in the central nucleus of the amygdala increases risk avoidance in exploratory tasks. Eneuro 9:1–12

De Bundel D, Zussy C, Espallergues J, Gerfen CR, Girault J-A, Valjent E (2016) Dopamine D2 receptors gate generalization of conditioned threat responses through mTORC1 signaling in the extended amygdala. Mol Psychiatry 21:1545–1553

De la Mora MP, Gallegos-Cari A, Crespo-Ramirez M, Marcellino D, Hansson AC, Fuxe K (2012) Distribution of dopamine D 2-like receptors in the rat amygdala and their role in the modulation of unconditioned fear and anxiety. Neuroscience 201:252–266

Dougalis AG, Matthews GAC, Bishop MW, Brischoux F, Kobayashi K, Ungless MA (2012) Functional properties of dopamine neurons and co-expression of vasoactive intestinal polypeptide in the dorsal raphe nucleus and ventro-lateral periaqueductal grey. Eur J Neurosci 36:3322–3332

Etkin A, Prater KE, Schatzberg AF, Menon V, Greicius MD (2009) Disrupted amygdalar subregion functional connectivity and

evidence of a compensatory network in generalized anxiety disorder. Arch Gen Psychiatry 66:1361–1372
Freedman LJ, Cassell MD (1994) Distribution of dopaminergic fibers in the central division of the extended amygdala of the rat. Brain Res 633:243–252
Giros B, Jaber M, Jones SR, Wightman RM, Caron MG (1996) Hyperlocomotion and indifference to cocaine and amphetamine in mice lacking the dopamine transporter. Nature 379:606–612
Greba Q, Gifkins A, Kokkinidis L (2001) Inhibition of amygdaloid dopamine D2 receptors impairs emotional learning measured with fear-potentiated startle. Brain Res 899:218–226
Groessl F, Munsch T, Meis S, Griessner J, Kaczanowska J, Pliota P et al (2018) Dorsal tegmental dopamine neurons gate associative learning of fear. Nat Neurosci 21:952–962
Gu Y, Piper WT, Branigan LA et al (2020) A brainstem-central amygdala circuit underlies defensive responses to learned threats. Mol Psychiatry 25:640–654
Guarraci FA, Frohardt RJ, Kapp BS (1999) Amygdaloid D1 dopamine receptor involvement in Pavlovian fear conditioning. Brain Res 827:28–40
Guarraci FA, Frohardt RJ, Falls WA, Kapp BS (2000) The effects of intra-amygdaloid infusions of a D2 dopamine receptor antagonist on Pavlovian fear conditioning. Behav Neurosci 114:647–651
Hasue RH, Shammah-Lagnado SJ (2002) Origin of the dopaminergic innervation of the central extended amygdala and accumbens shell: a combined retrograde tracing and immunohistochemical study in the rat. J Comp Neurol 454:15–33
Janak PH, Tye KM (2015) From circuits to behaviour in the amygdala. Nature 517:284–292
Jones SR, Gainetdinov RR, Wightman RM, Caron MG (1998) Mechanisms of amphetamine action revealed in mice lacking the dopamine transporter. J Neurosci 18:1979–1986
Kim J, Zhang X, Muralidhar S, LeBlanc SA, Tonegawa S (2017) Basolateral to central amygdala neural circuits for appetitive behaviors. Neuron 93:1464-1479.e5
Kim B, Yoon S, Nakajima R, Lee HJ, Lim HJ, Lee YK et al (2018) Dopamine D2 receptor-mediated circuit from the central amygdala to the bed nucleus of the *stria terminalis* regulates impulsive behavior. Proc Natl Acad Sci U S A 115:E10730–E10739
Koob GF (2008) A role for brain stress systems in addiction. Neuron 59:11–34
Koob GF, Volkow ND (2016) Neurobiology of addiction: a neurocircuitry analysis. The Lancet Psychiatry 3:760–773
Lammel S, Hetzel A, Häckel O, Jones I, Liss B, Roeper J (2008) Unique properties of mesoprefrontal neurons within a dual mesocorticolimbic dopamine system. Neuron 57:760–773
Lammel S, Steinberg EE, Földy C, Wall NR, Beier K, Luo L et al (2015) Diversity of transgenic mouse models for selective targeting of midbrain dopamine neurons. Neuron 85:429–438
Lamont EW, Kokkinidis L (1998) Infusion of the dopamine D1 receptor antagonist SCH 23390 into the amygdala blocks fear expression in a potentiated startle paradigm. Brain Res 795:128–136
Li C, Sugam JA, Lowery-Gionta EG, McElligott ZA, McCall NM, Lopez AJ et al (2016) Mu opioid receptor modulation of dopamine neurons in the periaqueductal gray/dorsal raphe: a role in regulation of pain. Neuropsychopharmacology 41:2122–2132
Madisen L, Zwingman TA, Sunkin SM, Oh SW, Hatim A, Gu H et al (2010) A robust and high-throughput Cre reporting and characterization. Nat Neurosci 13:133–140
McCullough KM, Morrison FG, Hartmann J, Carlezon WA, Ressler KJ (2018) Quantified co-expression analysis of central amygdala subpopulations. Eneuro. 5:0010–0018
Meloni EG (2006) Behavioral and anatomical interactions between dopamine and corticotropin-releasing factor in the rat. J Neurosci 26:3855–3863
National Research Council (2011) Guide for the care and use of laboratory animals: eighth edition. The National Academies Press, Washington, DC
Oh SW, Harris JA, Ng L, Winslow B, Cain N, Mihalas S et al (2014) A mesoscale connectome of the mouse brain. Nature 508:207–214
Olucha-Bordonau FE, Fortes-Marco L, Otero-García M, Lanuza E, Martínez-García F (2015) Amygdala: structure and function. The rat nervous system, 4th edn. Elsevier, pp 441–490
Paxinos G, Franklin K (2008) The mouse brain in stereotaxic coordinates, compact. Academic Press, San Diego, CA
Rueden CT, Schindelin J, Hiner MC, DeZonia BE, Walter AE, ArenaET EKW (2017) Image J2: imageJ for the next generation of scientific image data. BMC Bioinformatics 18:529
Schindelin J, Arganda-Carreras I, Frise E, Kaynig V, Longair M, Pietzsch T, Preibisch S, Rueden C, Saalfeld S, Schmid B, TinevezJY WDJ, Hartenstein V, Eliceiri K, Tomancak P, Cardona A (2012) Fiji: an open-source platform for biological-image analysis. Nat Methods 9:676–682
Stamatakis AM, Jennings JH, Ung RL, Blair GA, Weinberg RJ, Neve RL et al (2013) A unique population of ventral tegmental area neurons inhibits the lateral habenula to promote reward. Neuron 80:1039–1053
Stuber GD, Stamatakis AM, Kantak PA (2015) Considerations when using cre-driver rodent lines for studying ventral tegmental area circuitry. Neuron 85:439–445
Tye KM, Prakash R, Kim S-Y, Fenno LE, Grosenick L, Zarabi H et al (2011) Amygdala circuitry mediating reversible and bidirectional control of anxiety. Nature 471:358–362